Liquid Phase Exfoliated MoS_2 Nanosheets for High Volumetric/Areal Capacity Sodium-Ion Batteries

Yuping Liu,[1#] Xiaoyun He,[2#] Damian Hanlon, Andrew Harvey, Jonathan N. Coleman[2*] and Yanguang Li[1**]

[1]*Institute of Functional Nano & Soft Materials (FUNSOM), Jiangsu Key Laboratory for Carbon-Based Functional Materials and Devices, Soochow University, Suzhou 215123, China*

[2]*School of Physics, CRANN and AMBER Centers, Trinity College Dublin, Dublin 2, Ireland*

*colemaj@tcd.ie, **yanguang@suda.edu.cn [#]These authors contributed equally

ABSTRACT: The search for high capacity, low-cost electrode materials for sodium-ion batteries is a significant challenge in energy research. Among the many potential candidates, layered compounds such as MoS_2 have attracted increasing attention. However, such materials have not yet fulfilled their true potential. Here we show that networks of liquid phase exfoliated MoS_2 nanosheets, reinforced with 20 wt%, single-wall carbon nanotubes, can be formed into sodium-ion battery electrodes with large gravimetric, volumetric and areal capacity. The MoS_2/nanotube composite films are highly porous, electrically conductive and mechanically robust due to the percolating carbon nanotube network. When directly employed as the working electrode, they exhibit specific capacity of >400 mAh/g and volumetric capacity of ~650 mAh/cm^3. Their mechanical stability allows them to be processed into free-standing films with tunable thickness of up to ~100 μm, corresponding to an areal loading of 15 mg/cm^2. Their high electrical conductivity allows the high volumetric capacity to be retained, even at high thickness, resulting in state-of-the-art areal capacities of >6.0 mAh/cm^2. Such values are competitive with their lithium-ion counterparts.

KEYWORDS: liquid-phase exfoliation · MoS_2 nanosheets · sodium ion batteries · free-standing membranes · volumetric and areal capacities

Introduction

Lithium-ion batteries (LIBs) have been used as the main power source for portable electronics over the past two decades and are considered one of the most promising candidates for hybrid electric vehicles (HEVs) and electric vehicles (EVs).[1-4] However, concerns over the cost, availability and distribution of lithium in the earth's crust[5] have pushed researchers to develop new battery technologies based on more abundant and low-cost electrode materials.[6, 7] Among them, sodium-ion batteries (SIBs) have recently attracted intense interest owing to their similar insertion electrochemistry with their lithium-ion counterparts.[8-13] Nevertheless, before SIBs can become commercially competitive with LIBs, there are still a number of unsolved challenges.[11-14] For instance, Na ions are about 55% larger in radius than Li ions. This makes it difficult to find a suitable host material to accommodate Na ions, and to allow reversible and rapid ion insertion and extraction.

Recently, interest in transition metal dichalcogenides (TMDs) for efficient energy storage and conversion has been growing rapidly.[4, 15-18] These materials have unique two-dimensional layered structure analogous to graphite and consisting of covalently bonded monolayers brought together via weak van der Waals interactions. The most well studied example among them is MoS_2. Up to now, a variety of MoS_2-based materials have been exploited for LIBs with some encouraging success.[19-23] Because of the chemical similarity between Li^+ and Na^+, MoS_2-based materials have also been actively investigated for SIBs.[24-28] Nevertheless, their electrochemical performances as the anode materials of SIBs still falls short of expectations. Very few studies have been able to simultaneously achieve large capacity (>400 mAh/g), high rate capability (appreciable capacity at >10 A/g) and long cycling stability (>500 cycles) due to the larger size of Na^+ ions.[29, 30]

On the other hand, most current battery studies emphasize gravimetric capacities (C/M, mAh/g) but overlook other important metrics such as volumetric (C/V) and areal (C/A) capacities (mAh/cm^3 or mAh/cm^2). In many practical device applications, the volumetric capacities can be more important than gravimetric capacities, in particular for the portable devices where volume is more important than

weight.[31] For example, applications in HEVs and EVs require batteries to be not only light in weight but also compact in size. Furthermore, many battery architectures also require a high areal capacity which is related to electrode thickness (t) and volumetric capacity by $C/A = t \times C/V$. To achieve this, it requires an electrode material which can retain high volumetric capacity even at high electrode thickness. Unfortunately, the reported gravimetric capacities of most electrode materials in literature are usually achieved very low mass loadings of the active material, typically in the range of 0.5~2 mg/cm^2. This leads to optimistic capacity values that do not necessarily translate to high performance (high C/A) when comes to real batteries.[31] As a result, there is an urgent call to develop electrode materials with high volumetric/areal capacities and able to properly function at high mass loadings (> 5 mg/cm^2).[32-34]

Herein, we report the production of high-quality MoS_2 nanosheets dispersion with high yields using a facile liquid-phase exfoliation (LPE) technique.[35, 36] This method is insensitive to air and water, and can be conveniently scaled up to give large quantities of exfoliated material. The resultant dispersion is mixed with single wall nanotubes (SWNTs) to construct an MoS_2/SWNTs composite, which is highly porous, extremely conductive and mechanically robust.[23] Furthermore, as motivated by its high mechanical strength, we also prepare a flexible free-standing MoS_2/SWNTs membrane using vacuum filtration with tunable thickness up to 90 μm. This membrane can be directly employed as the working electrode of SIBs with an extremely high loading of active materials (up to 15 mg/cm^2) free of any binder, conducting additive or current collector. It achieves striking specific capacity (>400 mAh/g), volumetric capacity (~650 mAh/cm^3) as well as areal capacity (>6.0 mAh/cm^2).

Results and Discussion

Liquid phase exfoliation is a scalable and versatile process for producing mono-to few-layer nanosheets from a range of layered materials including graphite, TMDs and black phosphorus.[35] In solvents with surface tension closely matching the surface energy of these layered materials, prolonged

mechanical agitation by ultrasonic waves can result in their effective exfoliation at high yields. MoS_2 nanosheets were prepared by LPE of commercially sourced layered powders in N-methyl-pyrrolidone (NMP), which has previously been established as a good solvent for the LPE of MoS_2.[36] Figure 1a shows a photograph of a 250 mL bottle of MoS_2-NMP dispersion with a concentration of ~0.4 mg/mL. It is highly stable and can stand for several weeks without any obvious precipitates. The structure and phase of the exfoliated nanosheets were verified using multiple characterization techniques. The samples for transmission electron microscopy (TEM) were directly prepared from the dispersion. They are observed to be two-dimensional nanosheets with mostly few-layer thickness even though monolayers are also found (Figure 1b). From the high resolution TEM, it is evident that these nanosheets are highly crystalline and exhibit in-plane lattice fringes corresponding to the (100) plane of MoS_2 (Figure 1c). Selected area electron diffraction (SAED) pattern collected over a single nanosheet is featured with a set of six-fold diffraction spots, indicating each nanosheet is a high-quality single crystal with (001) termination. Statistical analysis based on TEM images suggests that the lateral size of nanosheets distributes over a broad range from ~100 nm to over 1 μm with a mean length around 300 nm (Figure 1d). In addition, the exfoliated product can be transferred to water and lyophilized to give powders of reaggregated nanosheets as depicted in the scanning electron microscopy (SEM) image in Figure 1e. Their XRD pattern matches well with that of 2H-MoS_2 without any noticeable impurity (Figure 1f).

Pristine MoS_2 nanosheet networks have poor intrinsic electrical conductivity and mechanical strength.[23, 35, 37] In order to address these problems for battery applications, they are usually reinforced with proper conductive additives such as graphene[19, 38] or carbon nanotubes.[39-41] Our recent work suggests that adding a small amount of SWNTs to MoS_2 nanosheets would result in up to $\times 10^{10}$ and ×40 times increases in electrical conductivity and mechanical toughness respectively, increases which are well described by the percolation theory.[23] In addition, SWNTs can also effectively prevent the re-stacking of MoS_2 nanosheets, thus increasing the accessibility of their high surface areas. Motivated

by these results, here we prepared MoS_2/SWNTs composite by physically mixing as-exfoliated MoS_2 nanosheets with 20 wt% nanotubes in isopropanol (IPA), transferring the composite to water, and finally lyophilizing it (see Experimental Methods). SEM images of the final composite at low and high magnification are displayed in Figure 2a,b. It can be clearly observed that MoS_2 nanosheets are uniformly dispersed within the percolating SWNT network (Figure 2b). Under TEM, individual MoS_2 nanosheets are found to be electrically wired with several SWNTs at the same time (Figure 2c). There is no evidence of macroscopic phase separation of these two components in the composite. Moreover, Raman spectroscopy unambiguously corroborates the presence of MoS_2 and SWNTs in the composite as shown in Figure 2d. The radial breathing mode (RBM) at ~164 cm^{-1} and the D, G and G´ bands at 1345, 1592, 2679 cm^{-1} respectively are associated with SWNTs; the two distinct peaks located at 379 and 402 cm^{-1} are characteristic to the E^1_{2g} and A_{1g} vibration modes of 2H-MoS_2.[42]

We next assessed the electrochemical performance of MoS_2/SWNTs composite as the SIB anode material. It was blended with polyacrylic acid binder, blade coated onto Cu foil, and then paired with a metallic Na disk in standard coin cells filled with 1 M $NaClO_4$ in 1:1 (v/v) ethylene carbonate (EC): diethylene carbonate (DEC) electrolyte. The areal loading of the active material was intentionally kept relatively low (~1 mg/cm^2) for this part of study to unveil its full potential and allow a reliable comparison with previous works reported in literature. Figure 3a depicts the cyclic voltammetry (CV) curves of MoS_2/SWNTs composite for the first three cycles. During the initial negative sweep, the CV curve exhibits two pronounced cathodic peaks centered at 0.85 V and 0.65 V (versus Na^+/Na, the same hereafter), followed by a broad cathodic wave down to the cutoff voltage. Based on the sodiation pathway of MoS_2, the two peaks are attributed to the stepwise intercalation of layered MoS_2 with Na^+ ions, whereas the broad wave in the deep cathodic process is contributed by the conversion of MoS_2 to form metallic Mo nanograins embedded in the Na_2S matrix, together with the irreversible formation of the solid electrolyte interface (SEI).[26] During the subsequent discharge, the original cathodic peaks totally vanish, and instead, two new peaks at 2.3 V and 1.1 V emerge. This observation is in a good

agreement with previous reports and indicative of permanent structural modification during the first cycle.[29, 43] All the positive-going CV curves exhibit four anodic peaks corresponding to multiple desodiation process.[26, 44] Consistent results are also garnered from the galvanostatic charge/discharge experiments at the specific current of 100 mA/g (Figure 3b). The discharge curve of the first cycle is featured with two distinct plateaus at 0.88 V and 0.73 V. However, its shape is dramatically altered in the following cycles as a result of the conversion reaction mechanism. The initial discharge capacity of MoS_2/SWNTs composite reaches ~770 mAh/g (normalized to the overall composite mass), and ~440 mAh/g can be recovered and reversibly sustained afterwards.

Figure 3c compares the cycling stability of MoS_2-only electrode and MoS_2/SWNTs composite electrode at the specific current of 200 mA/g. The specific capacity of the former quickly drops from 540 mAh/g at the second cycle to ~100 mAh/g at the end of 100 cycles. By stark contrast, the incorporation of percolating SWNT network in the latter significantly promotes its cycling performance. It starts at 410 mAh/g, and retains ~390 mAh/g after 100 cycles — corresponding to excellent capacity retention of ~95%. It is worth noting that the initial capacity value of the composite electrode is slightly lower than that of the MoS_2-alone electrode due to the incorporation of less electrochemically active SWNTs. Control experiments show that pure SWNTs only have a reversible specific capacity of ~90 mAh/g at 100 mA/g (Figure S1). Furthermore, MoS_2/SWNTs composite also demonstrates very impressive performance under large current rates. When the specific current is gradually ramped up, specific capacities of 437, 404, 370, 341, 302, 268 and 192 mAh/g are reversibly measured at 0.05, 0.2, 0.5, 1, 5, 10 and 20 A/g, respectively (Figure 3d). Among a handful of previous studies on MoS_2-based materials for SIBs, very few can attain >200 mAh/g at 10 A/g. The rate capability of our composite electrode clearly excels most of its competitors owing to its advantageous microstructure (Figure S2).[25, 28, 29, 45-48] Importantly, this does not come at the cost of inferior cycling stability under large current rates. In fact, the composite electrode can retain ~70% of its original capacity even after 1000 cycles at 500 mA/g (Figure 3e). This corresponds to a small average capacity

loss of 0.03% per cycle, and attests to its outstanding long-term cycling performance.

From above studies, it has been established that our MoS_2/SWNTs composite has the combination of large capacity, high rate capability and excellent cycling stability. We believe that its superior electrochemical performance is the collective effect of several structural factors as summarized below. Compared to chemical synthesis, MoS_2 nanosheets exfoliated by the LPE method have high quality[49] and are free of impurity.[36] These nanosheets are readily dispersible in IPA without the assistance of any surfactant, and can be uniformly mixed with SWNTs. The addition of 20 wt% SWNTs is beyond the electrical and mechanical percolation thresholds as shown in our previous study.[23] They form a three-dimensional percolating network, which not only provides a highly conductive pathway for the efficient charge transfer, but also mechanically reinforces the composite and accommodates the volume change upon extended charge and discharge cycling. Such a unique architecture of TMD nanosheets percolated with one-dimensional CNTs offers a great opportunity for high-performance Li^+ or Na^+ ion storage.

Despite its appealing specific capacity at the relatively low areal loading of ~1 mg/cm^2, we note that it does not necessarily translate to superior battery performance for real applications.[31, 33] This is because the specific capacity usually falls with increasing electrode thickness. There are a number of reasons for this. The most well-known is that electrolyte may not penetrate deep into a very thick electrode, and even if it does, the high rate performance may become diffusion-limited. In addition, for low conductivity electrode materials such as MoS_2, the thicker the electrode, the higher the resistance felt by an electron travelling from the current collector to a lithium storage site near the electrode surface. Again, this can limit performance at high rates. Less often considered is that, for mechanically poor materials such as nanosheet networks, the mechanical robustness of the electrode can fall with thickness.[50] This renders thick electrodes mechanically unstable and limits performance. These are significant problems for experimental materials as most commercial battery anodes require areal loading of 5~10 mg/cm^2 and thickness around 50-60 μm in order to have an appreciable energy

density.[51]

To resolve the problems described above, an anode material with certain properties is demanded. Maximizing the cell energy density requires maximizing the capacity of the electrode of a given area i.e. maximizing the areal capacity. Because $C/A = t \times C/V$, this requires a material which can display high volumetric capacity at large thickness. This shows that, in addition to specific or gravimetric capacities, volumetric and areal capacities are important battery metrics,[31, 33] which, unfortunately, have received far less attention than deserved in literature, in particular for SIBs. Retaining a high C/V at high thickness requires an electrode with porosity high enough to allow free access of the electrolyte and avoid diffusion limitations at high thickens, but not too high as this will result in reductions in volumetric capacity (for a given specific capacity). The material must also be electrically conductive enough to allow free access of electrons to all parts of the electrode. Finally, it must have mechanical properties (specifically toughness)[23] good enough to allow the electrode to be mechanically stable even when very thick.

We believe that nanosheet/carbon nanotube composites are ideal materials in these respects and perfect for producing high areal capacity SIB anodes. Such networks are highly conductive (up to 10^4 S/m) and mechanically strong and tough.[23] To this end, we went on to study the performance of our MoS_2/SWNTs composite at high areal loading, and to evaluate its volumetric and areal capacities. This was approached in an unconventional way. Inspired by the two-dimensional morphology of MoS_2 nanosheets and their mechanical reinforcement with SWNTs in the composite, we prepared MoS_2/SWNTs membranes by vacuum filtration (see Experimental Method). They can be easily peeled off from the filter membrane, and have sufficient mechanical strength and toughness to maintain the free-standing shape (Figure 4a). At the same time, they are flexible and can be curved without fracture as illustrated in Figure 4b. By controlling the volume of composite material during the vacuum filtration, we are able to tune the areal loading of MoS_2/SWNTs membranes from 2.5 mg/cm^2 up to 15 mg/cm^2. Their thickness is measured by a digital micrometer, and found to be in the range of 15-90

μm (Figure 4c). The packing density is then estimated to be ~1.7 g/cm^3, which remarkably exceeds those of most electrode materials reported in literature (< 1 g/cm^3).[52, 53] Moreover, taking the nanotube and MoS_2 densities to be 1.8 and 5.1 g/cm^3 respectively allows us to estimate the porosity as ~50%. This should easily be sufficient to allow access of the electrolyte throughout the network. Figure 4d selectively shows the cross-section SEM image of a membrane with the areal loading of 5 mg/cm^2. Its thickness is largely uniform and determined to be around 30 μm. Close examination reveals that the membrane is consisted of MoS_2 nanosheets densely stacked together and infiltrated with interconnected SWNTs, in a brick-and-mortar-like arrangement (Figure 4e).

These free-standing MoS_2/SWNTs membranes were directly employed as the electrode film for SIBs without any additional binder or current collector. This is possible only because of the high conductivity and mechanical performance of these composites. They were galvanostatically charged and discharged at an areal current of 0.2 mA/cm^2. Capacities were normalized to the membrane mass, volume or geometric area. As shown in Figure 5a, all thicknesses deliver very similar initial gravimetric and volumetric capacities, with values between 393-420 mAh/g and 655-700 mAh/cm^3 respectively. Their areal capacities were found to linearly scale with thickness (and so areal loading), exceeding 6 mAh/cm^2 for the 93 μm membrane, consistent with a volumetric capacity of C/V = 650 mAh/cm^3 (Figure 5b-c). This suggests that the entire membranes are effectively utilized in the battery reaction as the result of improved electrical conductivity of the composite afforded by the SWNT percolation as well as the intrinsic porosity of the electrodes. The 15, 30 and 52 μm thick electrodes display excellent stability with virtually no capacity loss after 100 cycles. However, further increasing the membrane thickness (Figure 5a,b,c) results in inferior cycling stability with an areal capacity of only ~3.7 mAh/cm^2 at the end of 100 cycles for the 72 μm thick electrode. This leads us to conclude that the practical upper limit of the membrane thickness probably lies between 50~70 μm, beyond which the electrochemical performance of MoS_2/SWNTs membranes starts to be compromised. It can be seen in Figure 5d where we examine the electrode stability by plotting the capacity retention from

N = 2 to N = 100 cycles versus electrode thickness. The data clearly show very good capacity retention for electrodes with t ≤ 52 μm but a dramatic fall off in stability for thicker electrodes.

As far as we know, there are no previous reports on the areal or volumetric capacities of any SIB electrode materials. However, the significance of our results can be grasped from the comparison with LIB electrode materials. For example, commercial graphite electrode for LIBs has a volumetric or areal capacity of ~550 mAh/cm^3 or ~4 mAh/cm^2 respectively;[32] the best Si-based materials have areal capacities < 3 mAh/cm^2;[54] two-dimensional transition metal carbides (MXenes) have been recently reported to have reversible volumetric or areal capacities up to 264 mAh/cm^3 and 6.7 mAh/cm^2 respectively.[33] It is worth emphasizing that electrode materials usually have much smaller storage capacity for Na^+ ions than for Li^+ ions.[11, 13] As a result, the reversible volumetric capacities of 655-700 mAh/cm^3 and the areal capacities ~4 mAh/cm^2 reported in this work for SIBs are truly remarkable. This would not be possible if it wasn't for the combination of high electrochemical activity, excellent electrical and mechanical properties and compact size of MoS_2/SWNTs membranes, and reflect the great potential of our materials in practical applications.

Conclusions

In summary, we prepared high-quality MoS_2 nanosheets in a large quantity using the facile LPE method. They were mixed with 20 wt% SWNTs to afford a composite with high porosity, excellent electrical conductivity and mechanical robustness. When evaluated as the SIB anode material at the normal condition, the composite material exhibited large specific capacity and great long-term cycling stability under both low and high current rates. More importantly, we demonstrated that the composite material could be readily processed into flexible and free-standing membranes with tunable thickness via the vacuum filtration, and directly utilized as the battery electrode without any binder or current collector. They achieved striking specific capacity of >400 mAh/g, volumetric capacity of ~650 mAh/cm^3 as well as areal capacity of up to >6.0 mAh/cm^2. Our study here represents the first

experimental report on the volumetric or areal capacities of SIB electrode materials as far as we are aware. These values are outstanding, and even superior to those of most LIB electrode materials, as enabled by the hierarchical architecture percolated with the SWNT network. We believe our strategy of combined LPE and vacuum filtration could be extended to the preparation of other TMD composite membranes for high volumetric/areal capacity sodium-ion storage.

Acknowledgement: We thank the National Natural Science Foundation of China (51472173 and 51522208), the Natural Science Foundation of Jiangsu Province (BK20140302 and SBK2015010320), Science Foundation Ireland (11/PI/1087), the European Research Council (SEMANTICS), the European Union Seventh Framework Program under grant agreement n° 604391 (Graphene Flagship) for financial support. We acknowledge support from the Collaborative Innovation Centre of Suzhou Nano Science, the Priority Academic Program Development of Jiangsu Higher Education Institutions and Technology, and the SFI-funded AMBER research centre (SFI/12/RC/2278).

Experimental Section

Materials

Molybdenum (IV) sulphide powder (MoS_2, 99%), 1-Methyl-2-pyrrolidinone (NMP, ≥ 99%) and 2-propanol (IPA, ≥99.9%) were obtained from Sigma-Aldrich (Dublin, Ireland). P3-SWNT (CNT, > 90%) was purchased from Carbon Solutions, Inc.

Preparation of MoS_2/SWNTs composite and free-standing membranes

MoS_2 nanosheet dispersion was obtained by the LPE of MoS_2 bulk powders in NMP bath for 4 h using a horn-probe tip sonicator (Sonics Vibra-cell VCX-750W ultrasonic processor) operating at 60% amplitude and 6 s on and 2 s off pulse while ice-cooling the dispersion. The resultant raw dispersion was centrifuged for 60 min at 1000 rpm to remove unexfoliated MoS_2. Subsequently, the supernatant

was decanted and centrifuged for 90 min at 4500 rpm. Sediments were collected and redispersed in IPA to form a nanosheet dispersion of 0.4 mg/mL using a sonic bath. To prepare MoS_2/SWNTs composite, SWNTs were added into IPA, and sonicated for 60 min at 40% amplitude to forme a dispersion of 0.1 mg/mL. The MoS_2 nanosheet dispersion from above was then mixed with the SWNT dispersion in 1:1 volume ratio, and sonicated for another 30 min. 20% MoS_2/SWNTs composite powders were collected by centrifugation for 60 min at 8000 rpm, washed with H_2O and finally lyophilized. Free-standing MoS_2/SWNTs membranes were prepared by the direct vacuum filtration of the calculated volume of MoS_2/SWNTs IPA dispersion through a polyester membrane with a pore size of 200 nm. The resultant composite membranes were naturally dried, and then carefully peeled off from the filter.

Characterization

SEM images were obtained using a Zeiss Ultra Plus. TEM imaging was performed on FEI TecnaiG^2 F20 transmission electron microscope operated at 200 kV. Statistical analysis of TEM was preformed of the flake dimensions by measuring the longest axis of each nanosheet and assigning it as the length followed by measuring an axis perpendicular to this at its widest point and assigning it as the width. Raman spectroscopy was carried out on Horiba Jobin Yvon LabRAM HR800 with 532 nm excitation laser wavelength.

Battery Electrode Preparation

For regular coin cell measurements, the MoS_2/SWNTs composite was mixed with polyacrylic acid in 9:1 weight ratio, and dispersed in H_2O to form homogeneous slurry. It was subsequently blade coated onto Cu foil, and vacuum dried at 60 ^oC for 24 h. Standard CR2032 coin cells were assembled in an argon-filled glovebox by pairing the working electrode with a metallic Na disk, separated by Celgard 2400 polypropylene membrane and filled with 1 M $NaClO_4$ in 1:1 v/v ethylene carbonate (EC)/diethyl

carbonate (DEC) electrolyte. Galvanostatic charge/discharge measurements were carried out on a MTI Battery Testing System (CT-3008) between 3.0 and 0.1 V at room temperature. CV curves were collected on a CHI660E potentiostat at a scan rate of 0.2 mV/s. For experiments involving the free-standing MoS_2/SWNTs membranes, they were directly employed as the working electrode without the addition of any binder or current collector under otherwise similar condition.

Reference

[1] M. Armand, J. M. Tarascon, *Nature* **2008**, 451, 652.

[2] K. S. Kang, Y. S. Meng, J. Breger, C. P. Grey, G. Ceder, *Science* **2006**, 311, 977.

[3] V. Etacheri, R. Marom, R. Elazari, G. Salitra, D. Aurbach, *Energy Environ. Sci.* **2011**, 4, 3243.

[4] J. B. Goodenough, *Accounts Chem. Re.s* **2013**, 46, 1053.

[5] G. M. Clarke, *Chem. Eng. Prog.* **2013**, 109, 44.

[6] Y. G. Li, H. J. Dai, *Chem. Soc. Rev.* **2014**, 43, 5257.

[7] M. C. Lin, M. Gong, B. G. Lu, Y. P. Wu, D. Y. Wang, M. Y. Guan, M. Angell, C. X. Chen, J. Yang, B. J. Hwang, H. J. Dai, *Nature* **2015**, 520, 325.

[8] H. L. Pan, Y. S. Hu, L. Q. Chen, *Energy Environ. Sci.* **2013**, 6, 2338.

[9] W. Luo, F. Shen, C. Bommier, H. L. Zhu, X. L. Ji, L. B. Hu, *Accounts Chem. Res.* **2016**, 49, 231.

[10] X. D. Xiang, K. Zhang, J. Chen, *Adv. Mater.* **2015**, 27, 5343.

[11] N. Yabuuchi, K. Kubota, M. Dahbi, S. Komaba, *Chem. Rev.* **2014**, 114, 11636.

[12] D. Kundu, E. Talaie, V. Duffort, L. F. Nazar, *Angew. Chem. Int. Edit.* **2015**, 54, 3431.

[13] S. Y. Hong, Y. Kim, Y. Park, A. Choi, N.-S. Choi, K. T. Lee, *Energy Environ. Sci.* **2013**, 6, 2067.

[14] V. L. Chevrier, G. Ceder, *J. Electrochem. Soc.* **2011**, 158, A1011.
[15] R. Lv, J. A. Robinson, R. E. Schaak, D. Sun, Y. Sun, T. E. Mallouk, M. Terrones, *Accounts. Chem. Res.* **2015**, 48, 56.
[16] Q. Lu, Y. Yu, Q. Ma, B. Chen, H. Zhang, *Adv. Mater.* **2016**, 28, 1917.
[17] J. Jin, Z. Q. Shi, C. Y. Wang, *Electrochim. Acta* **2014**, 141, 302.
[18] Y. P. Liu, H. T. Wang, L. Cheng, N. Han, F. P. Zhao, P. R. Li, C. H. Jin, Y. G. Li, *Nano Energy* **2016**, 20, 168.
[19] K. Chang, W. X. Chen, *ACS Nano* **2011**, 5, 4720.
[20] L. C. Yang, S. N. Wang, J. J. Mao, J. W. Deng, Q. S. Gao, Y. Tang, O. G. Schmidt, *Adv. Mater.* **2013**, 25, 1180.
[21] T. Stephenson, Z. Li, B. Olsen, D. Mitlin, *Energy Environ. Sci.* **2014**, 7, 209.
[22] J. W. Zhou, J. Qin, X. Zhang, C. S. Shi, E. Z. Liu, J. J. Li, N. Q. Zhao, C. N. He, *ACS Nano* **2015**, 9, 3837.
[23] Y. P. Liu, X. Y. He, D. Hanlon, A. Harvey, U. Khan, Y. G. Li, J. N. Coleman, *ACS Nano In Press* **2016**.
[24] K. Chang, D. S. Geng, X. F. Li, J. L. Yang, Y. J. Tang, M. Cai, R. Y. Li, X. L. Sun, *Adv. Energy Mater.* **2013**, 3, 839.
[25] Z. Hu, L. X. Wang, K. Zhang, J. B. Wang, F. Y. Cheng, Z. L. Tao, J. Chen, *Angew. Chem. Int. Edit.* **2014**, 53, 12794.
[26] L. David, R. Bhandavat, G. Singh, *ACS Nano* **2014**, 8, 1759.
[27] J. J. Wang, C. Luo, T. Gao, A. Langrock, A. C. Mignerey, C. S. Wang, *Small* **2015**, 11, 473.
[28] X. Q. Xie, Z. M. Ao, D. W. Su, J. Q. Zhang, G. X. Wang, *Adv. Funct. Mater.* **2015**, 25, 1393.
[29] S. H. Choi, Y. N. Ko, J.-K. Lee, Y. C. Kang, *Adv. Funct. Mater.* **2015**, 25, 1780.
[30] Y. Y. Lu, Q. Zhao, N. Zhang, K. X. Lei, F. J. Li, J. Chen, *Adv. Funct. Mater.* **2016**, 26, 911.
[31] Y. Gogotsi, P. Simon, *Science* **2011**, 334, 917.
[32] J. M. Luo, X. Y. Tao, J. Zhang, Y. Xia, H. Huang, L. Y. Zhang, Y. P. Gan, C. Liang, W. K. Zhang, *Acs Nano* **2016**, 10, 2491.
[33] S. J. Kim, M. Naguib, M. Q. Zhao, C. F. Zhang, H. T. Jung, M. W. Barsoum, Y. Gogotsi, *Electrochim. Acta* **2015**, 163, 246.
[34] X. Wang, L. Lv, Z. Cheng, J. Gao, L. Dong, C. Hu, L. Qu, *Adv. Energy Mater.* **2016**, 6, n/a.
[35] J. N. Coleman, M. Lotya, A. O'Neill, S. D. Bergin, P. J. King, U. Khan, K. Young, A. Gaucher, S. De, R. J. Smith, I. V. Shvets, S. K. Arora, G. Stanton, H. Y. Kim, K. Lee, G. T. Kim, G. S. Duesberg, T. Hallam, J. J. Boland, J. J. Wang, J. F. Donegan, J. C. Grunlan, G. Moriarty, A. Shmeliov, R. J. Nicholls, J. M. Perkins, E. M. Grieveson, K. Theuwissen, D. W. McComb, P. D. Nellist, V. Nicolosi, *Science* **2011**, 331, 568.
[36] K. R. Paton, E. Varrla, C. Backes, R. J. Smith, U. Khan, A. O'Neill, C. Boland, M. Lotya, O. M. Istrate, P. King, T. Higgins, S. Barwich, P. May, P. Puczkarski, I. Ahmed, M. Moebius, H. Pettersson, E. Long, J. Coelho, S. E. O'Brien, E. K. McGuire, B. M. Sanchez, G. S. Duesberg, N. McEvoy, T. J. Pennycook, C. Downing, A. Crossley, V. Nicolosi, J. N. Coleman, *Nat. Mater.* **2014**, 13, 624.
[37] G. Cunningham, D. Hanlon, N. McEvoy, G. S. Duesberg, J. N. Coleman, *Nanoscale* **2015**, 7, 198.
[38] X. H. Cao, Y. M. Shi, W. H. Shi, X. H. Rui, Q. Y. Yan, J. Kong, H. Zhang, *Small* **2013**, 9, 3433.
[39] Y. M. Shi, Y. Wang, J. I. Wong, A. Y. S. Tan, C. L. Hsu, L. J. Li, Y. C. Lu, H. Y. Yang, *Sci. Rep.* **2013**, 3.
[40] C. B. Zhu, X. K. Mu, P. A. van Aken, J. Maier, Y. Yu, *Adv. Energy Mater.* **2015**, 5.
[41] J. Z. Wang, L. Lu, M. Lotya, J. N. Coleman, S. L. Chou, H. K. Liu, A. I. Minett, J. Chen, *Adv. Energy Mater.* **2013**, 3, 798.
[42] M. Boukhicha, M. Calandra, M.-A. Measson, O. Lancry, A. Shukla, *Phys. Rev. B: Condens. Matter Mater. Phys.* **2013**, 87, 195316/1.
[43] X. Q. Xiong, W. Luo, X. L. Hu, C. J. Chen, L. Qie, D. F. Hou, Y. H. Huang, *Sci. Rep.* **2015**, 5.
[44] C. B. Zhu, X. K. Mu, P. A. van Aken, Y. Yu, J. Maier, *Angew. Chem. Int. Edit.* **2014**, 53, 2152.
[45] G. S. Bang, K. W. Nam, J. Y. Kim, J. Shin, J. W. Choi, S.-Y. Choi, *ACS Appl. Mater. Interfaces* **2014**, 6, 7084.
[46] Y.-X. Wang, K. H. Seng, S.-L. Chou, J.-Z. Wang, Z. Guo, D. Wexler, H.-K. Liu, S.-X. Dou, *Chem. Commun.* **2014**, 50, 10730.

[47] Y.-X. Wang, S.-L. Chou, D. Wexler, H.-K. Liu, S.-X. Dou, *Chem. - Eur. J.* **2014**, 20, 9607.
[48] X. Wang, Y. Li, Z. Guan, Z. Wang, L. Chen, *Chem. - Eur. J.* **2015**, 21, 6465.
[49] C. Backes, B. M. Szydlowska, A. Harvey, S. Yuan, V. Vega-Mayoral, B. R. Davies, P.-l. Zhao, D. Hanlon, E. J. G. Santos, M. I. Katsnelson, W. J. Blau, C. Gadermaier, J. N. Coleman, *ACS Nano* **2016**, 10, 1589.
[50] T. M. Higgins, D. McAteer, J. C. M. Coelho, B. M. Sanchez, Z. Gholamvand, G. Moriarty, N. McEvoy, N. C. Berner, G. S. Duesberg, V. Nicolosi, J. N. Coleman, *ACS Nano* **2014**, 8, 9567.
[51] M. Singh, J. Kaiser, H. Hahn, *J Electrochem Soc* **2015**, 162, A1196.
[52] D. C. Lin, Z. D. Lu, P. C. Hsu, H. R. Lee, N. Liu, J. Zhao, H. T. Wang, C. Liu, Y. Cui, *Energ Environ Sci* **2015**, 8, 2371.
[53] P. Simon, Y. Gogotsi, *Accounts Chem. Res.* **2013**, 46, 1094.
[54] T. M. Higgins, S.-H. Park, P. J. King, C. Zhang, N. McEvoy, N. C. Berner, D. Daly, A. Shmeliov, U. Khan, G. Duesberg, V. Nicolosi, J. N. Coleman, *ACS Nano* **2016**, 10, 3702.

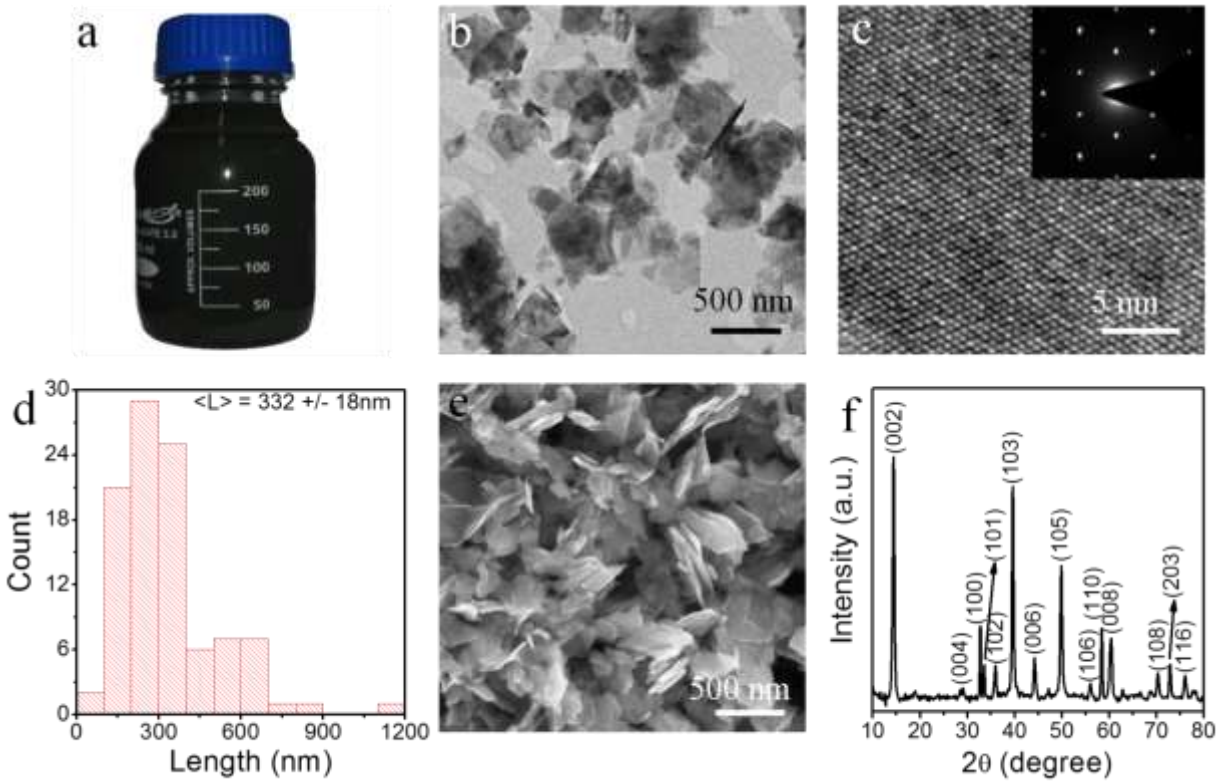

Figure 1. Liquid-phase exfoliated MoS_2 nanosheets. (a) Photograph of an as-prepared MoS_2 nanosheet dispersion in NMP; (b,c) TEM images of exfoliated MoS_2 nanosheets, insert in (c) is the corresponding SAED pattern; (d) histogram of the lateral size distribution of exfoliated MoS_2 nanosheets by TEM statistics; (e) SEM and (f) XRD pattern of aggregated MoS_2 nanosheets.

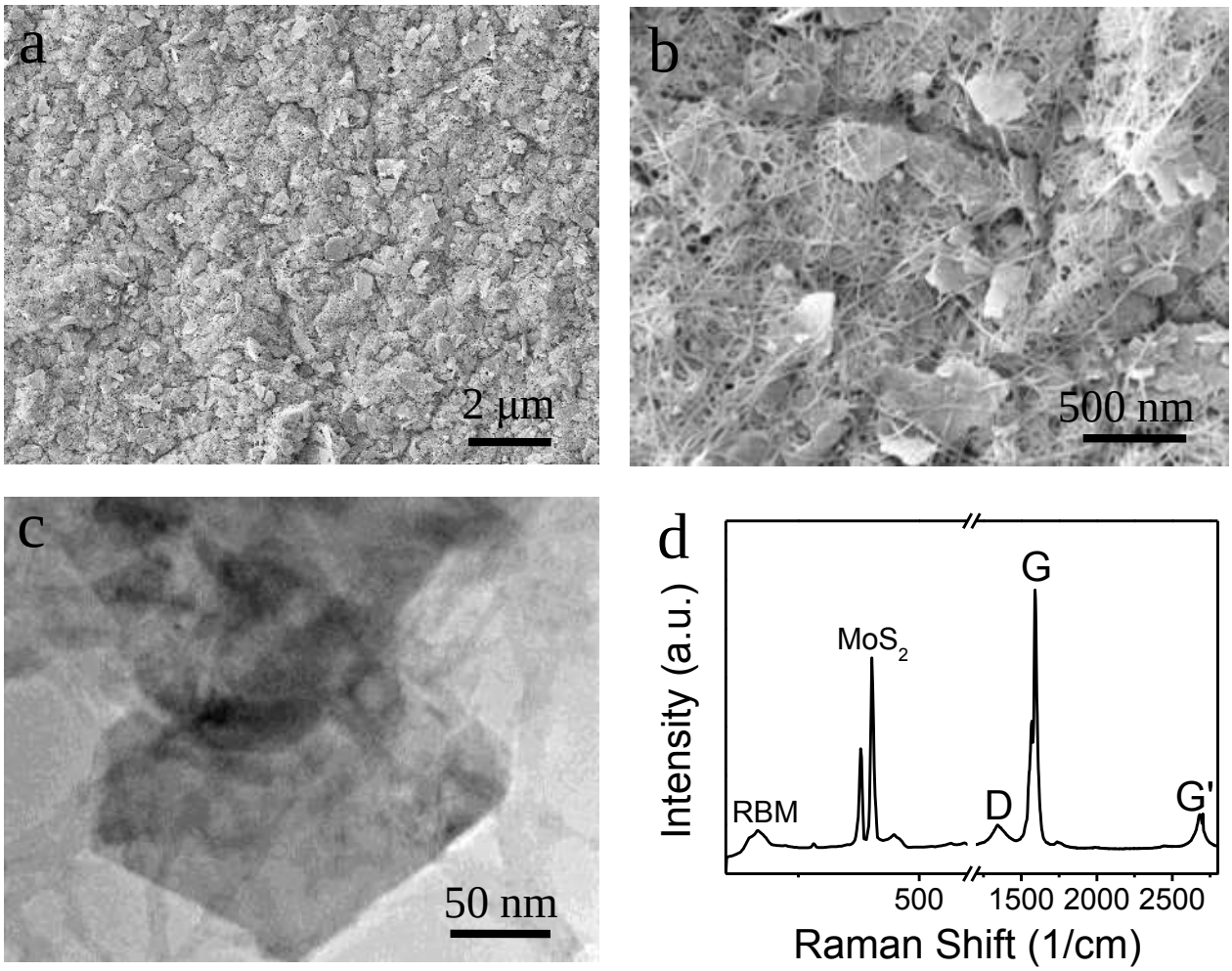

Figure 2. Morphology and composition analysis of MoS_2/SWNTs composite. (a,b) SEM images, (c) TEM image, and (d) Raman spectrum of the MoS_2/SWNTs composite.

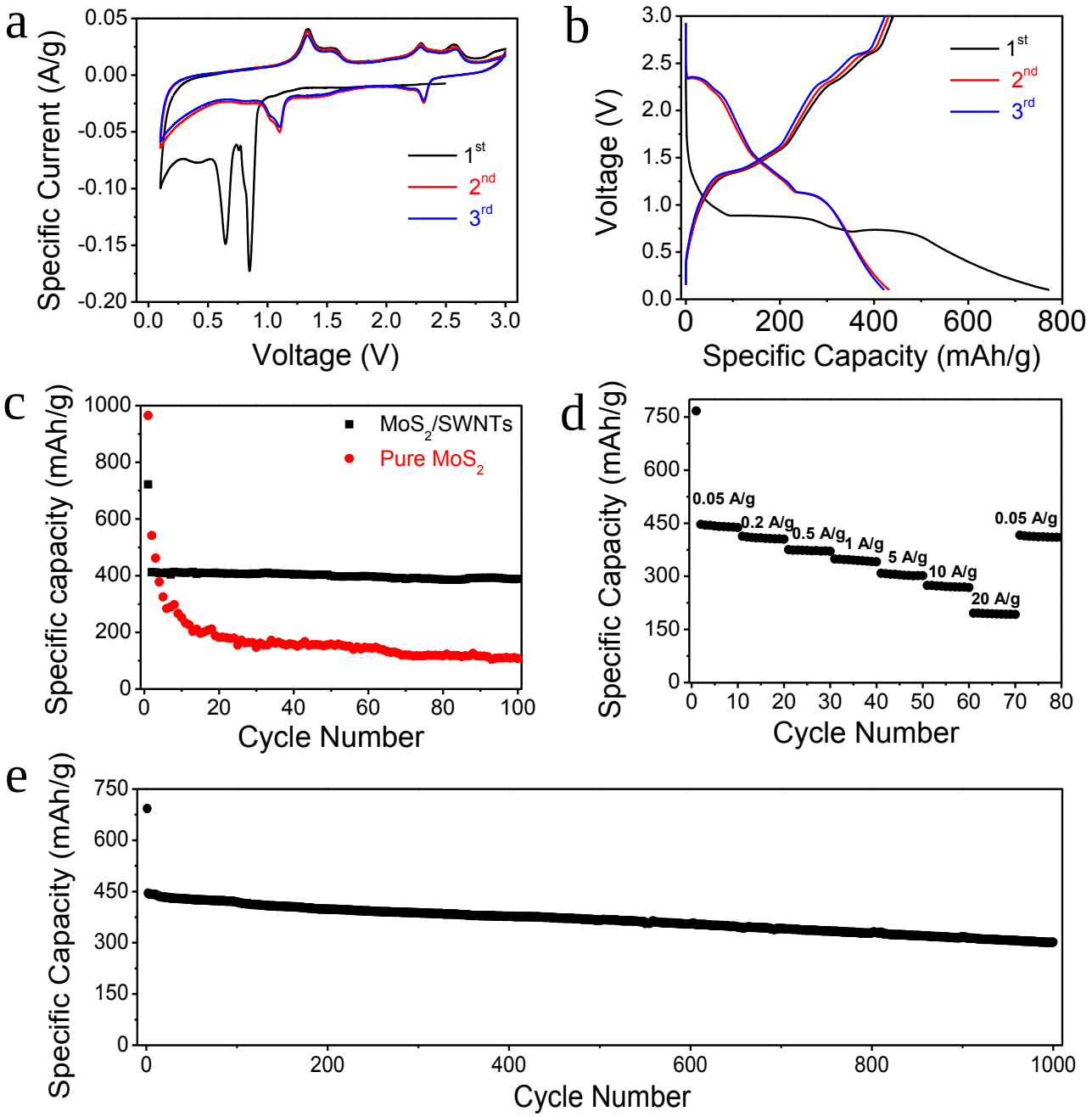

Figure 3. Electrochemical measurements of MoS_2/SWNTs composite as the SIB anode material. (a) CV curves for the first three cycles at the scan rate of 0.2 mV/s; (b) galvanostatic charge/discharge curves of MoS_2/SWNTs electrode for the first three cycles at 100 mA/g; (c) cycling stability of MoS_2/SWNTs at 200 mA/g in comparison with MoS_2-alone electrode; (d) rate capability of MoS_2/SWNTs at different specific currents as indicated; (e) long-term cycling stability of the MoS_2/SWNTs composite at 500 mA/g.

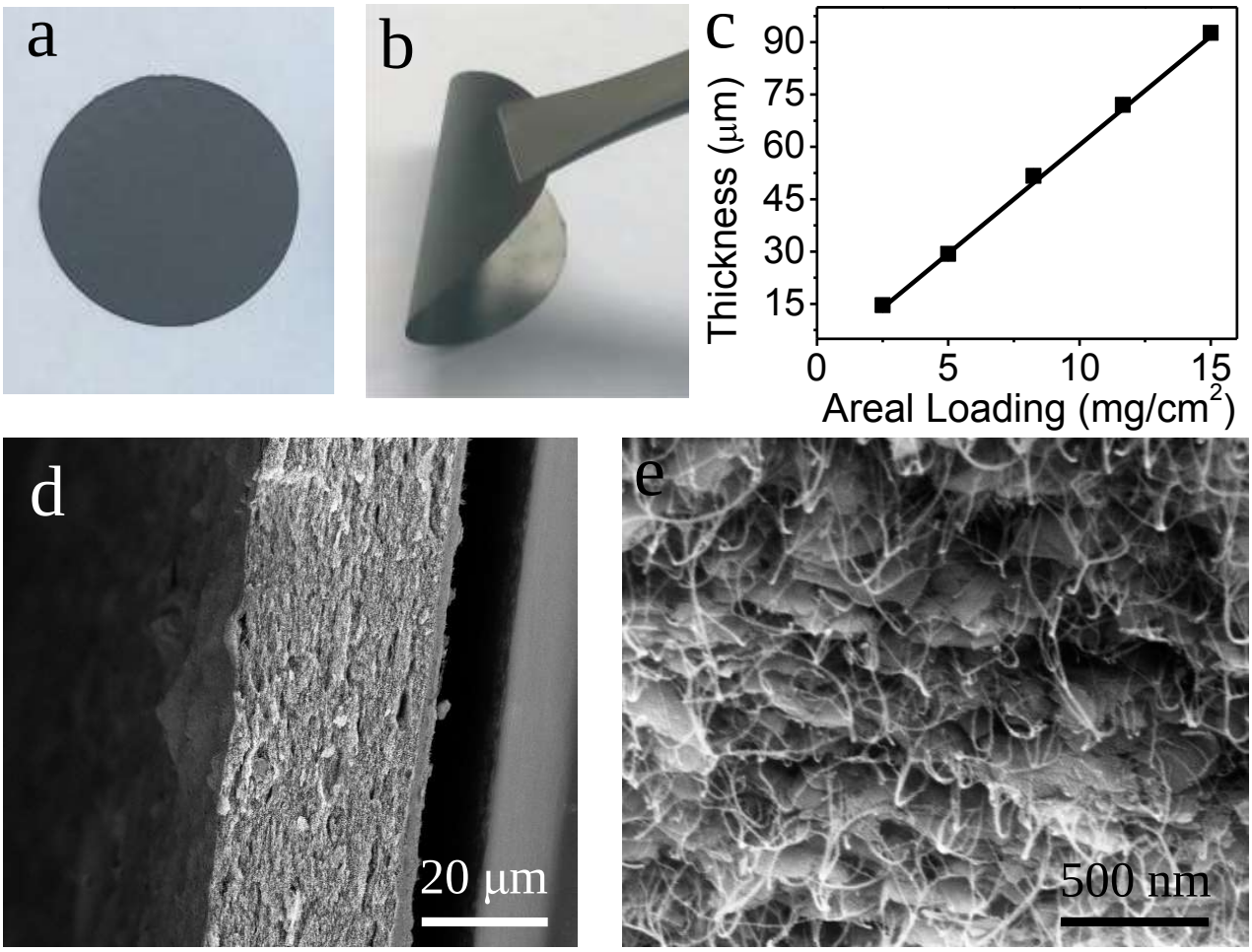

Figure 4. Fabrication of free-standing MoS_2/SWNTs composite membranes. (a-b) Photos of the MoS_2/SWNTs membrane; (c) areal loading versus thickness plot for the MoS_2/SWNTs membrane; (d,e) cross-section SEM images of the MoS_2/SWNTs membrane at different magnifications.

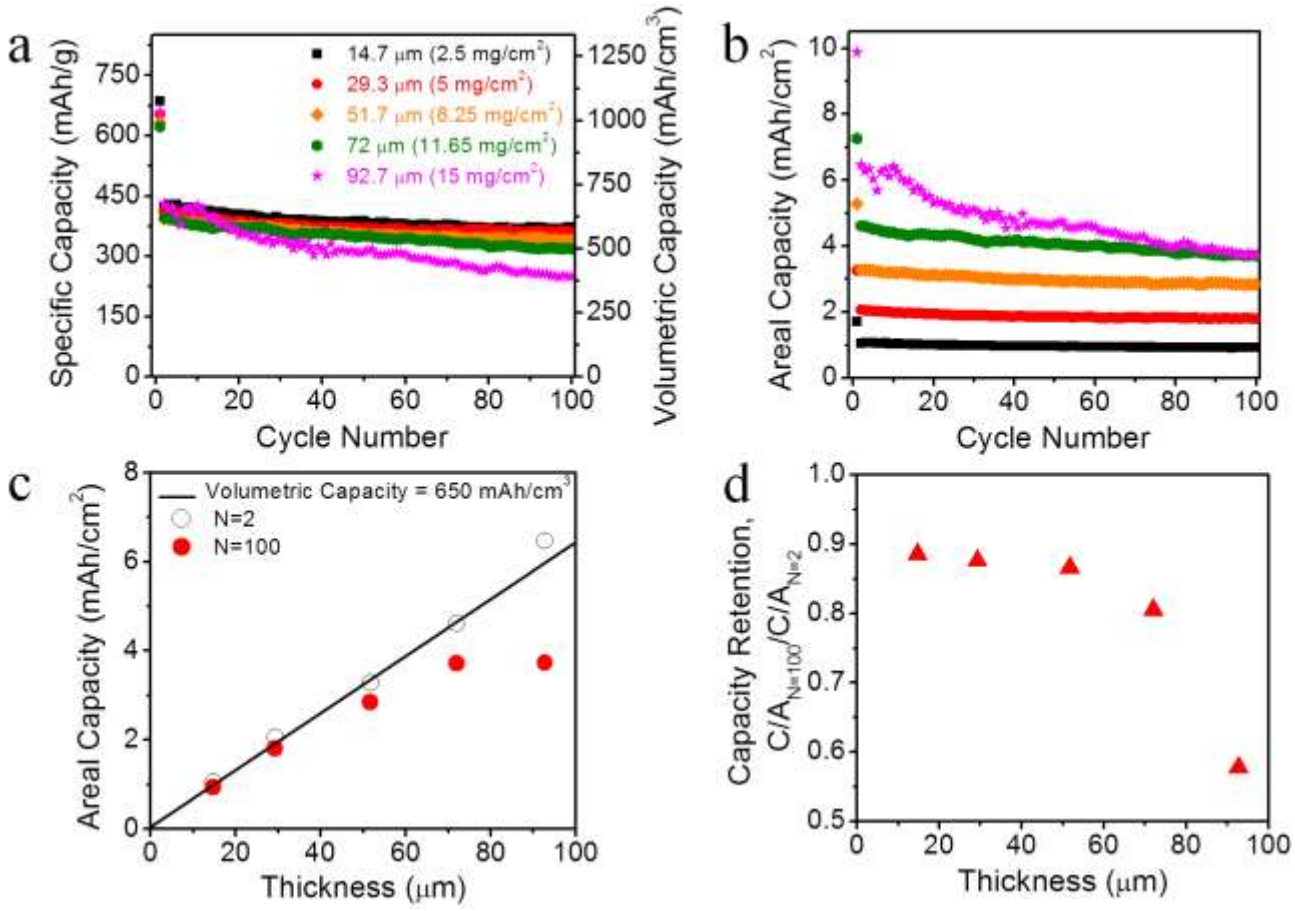

Figure 5. Electrochemical measurements of free-standing MoS_2/SWNTs membranes without additional binder or current collector. (a) Specific capacities and volumetric capacities of MoS_2/SWNTs membranes with different thicknesses as indicated; (b) areal capacities of MoS_2/SWNTs membranes with different thicknesses as indicated, the legend in (a) also applies to (b); (c) areal capacity measured on both the 2nd and 100th cycle plotted versus electrode thickness, the line represents the behavior expected for a volumetric capacity of 650 mAh/cm^3; and (d) capacity retention, defined as the ratio of capacity after 100 cycles to that after 2 cycles, plotted versus electrode thickness. All the experiments here were done at the areal current of 0.2 mA/cm^2.